


Extending bandwidth sensitivity of Rydberg-atom-based microwave electrometry using an auxiliary microwave field

Yue Cui , Feng-Dong Jia,^{*} Jian-Hai Hao , Yu-Han Wang , Fei Zhou, and Xiu-Bin Liu
School of Physical Sciences, University of Chinese Academy of Sciences, Beijing 100049, China


Yong-Hong Yu and Jiong Mei
School of Physical Sciences, University of Chinese Academy of Sciences, Beijing 100049, China
and Institute of Physics, Chinese Academy of Sciences, Beijing 100190, China

Jin-Hai Bai, Ying-Ying Bao, Dong Hu, and Yu Wang
Science and Technology on Metrology and Calibration Laboratory, Changcheng Institute of Metrology & Measurement, Aviation Industry Corporation of China, Beijing 100095, China

Ya Liu
National Time Service Centre, Chinese Academy of Sciences, Xi'an 710600, China
and University of Chinese Academy of Sciences, Beijing 100049, China

Jian Zhang and Feng Xie [†]
Institute of Nuclear and New Energy Technology, Collaborative Innovation Center of Advanced Nuclear Energy Technology, Key Laboratory of Advanced Reactor Engineering and Safety of Ministry of Education, Tsinghua University, Beijing 100084, China

Zhi-Ping Zhong
School of Physical Sciences, University of Chinese Academy of Sciences, Beijing 100049, China
and CAS Center for Excellence in Topological Quantum Computation, University of Chinese Academy of Sciences, Beijing 100190, China

 (Received 4 November 2022; revised 18 January 2023; accepted 20 March 2023; published 3 April 2023)

We demonstrate the use of an auxiliary microwave field to extend the bandwidth sensitivity of Rydberg-atom-based microwave electrometry. Electromagnetically induced transparency (EIT) and Autler-Townes (AT) splitting in Rydberg atom microwave electrometry provide advantageous sensitivity for the resonant detection of microwave (MW) fields because the Stark shift of the target Rydberg state takes the linear form of AT splitting. However, the sensitivity is reduced by several orders of magnitude for detuned MW fields because the Stark shift of the target Rydberg state depends on a weak nonlinear effect. We show that the auxiliary microwave field with appropriate Rabi frequency or detuning could shift the atomic energy levels to bring a particular Rydberg-Rydberg transition of interest for microwave sensing into resonance with the target microwave field. Using the atomic superheterodyne method, we verified the general method that regulates Rydberg energy levels using an auxiliary microwave field. The experimental results of this study confirm that this technique works efficiently for detecting microwave fields detuned by up to 100 MHz from resonance with the field-free Rydberg-Rydberg transition used for sensing. The measurement sensitivity of the detuned target field is increased by a factor of 10 compared with that achieved without the application of the auxiliary dressing field.

DOI: [10.1103/PhysRevA.107.043102](https://doi.org/10.1103/PhysRevA.107.043102)

I. INTRODUCTION

Quantum sensors [1] are based on a theoretical framework of quantum mechanics. By exploiting the quantum effects in atoms and photons to perform precise measurements of various physical quantities [2–11], the measurement results can be traced back to basic physical constants to achieve improved measurement sensitivity and precision compared to those of conventional sensors [2,10–18].

The advent of quantum sensors more than 100 years after the invention of the conventional dipole antenna has transformed microwave electric-field measurements [19]. Room-temperature quantum sensors for microwave electric fields have great potential for microwave (MW) communications, sensing, and metrology [1,20–24]. In particular, unlike conventional antennas, the frequency bandwidth of a Rydberg atomic microwave electric field sensor is not limited by antenna geometry [19]. A measurable finite-frequency broadband [19,25,26] covering MHz to THz frequencies can be achieved by (a) choosing Rydberg states with different principal quantum numbers n and (b) by exploiting the linear proportionality between the electromagnetically induced

^{*}fdjia@ucas.ac.cn

[†]fxie@tsinghua.edu.cn

transparency (EIT)-Autler-Townes (AT) splitting interval and the microwave electric field strength [27]. Although potentially hundreds of resonance transitions between Rydberg energy levels exist, linear measurement can only be achieved within several MHz around a single resonance transition. Achieving electric field measurements across a continuous frequency range requires multiple resonance transitions, which impose stringent demands on the laser system [25] and make it difficult to realize continuous broadband Rydberg atomic sensors in microwave electric fields. Expanding the linear response range of each available Rydberg-level transition in Rydberg sensors is a key requirement for obtaining reliable linear responses in continuous-frequency broadband microwave electric field measurements.

To expand the bandwidth of Rydberg atomic microwave electric field sensors to measure MW fields across a wider frequency range, various external fields have been added to produce energy-level shifting effects on the target energy level [28–33]. By adding a static magnetic field of 0–50 G, the Rydberg EIT system produces energy level shifts from the linear Zeeman effect to the quadratic Zeeman and Paschen-Back effects, causing a complex spectral structure [29] and making the MW measurement more difficult. The Rydberg energy level can be changed through the Stark effect in the system, induced by applying a static electric field. The second-order Stark shift in the low-angular momentum Rydberg state allows frequencies in nonresonant regions to be measured such that a wide microwave field spectral range from a few MHz to 1 GHz can be detected simultaneously [30]. However, applying a static electric or magnetic field to the system changes all atomic energy levels [29,30], causing significant theoretical and experimental difficulties. The detuned field can be detected, and the lower limit of measurement can be extended using two-photon resonance AT splitting, which is caused by an auxiliary microwave field that is nearly resonant with the adjacent Rydberg transition [32]. A different approach for achieving highly sensitive measurements in the nonresonant region is to introduce a local (LO) microwave field with a frequency close to that of the signal (SIG) microwave field using a nonresonant heterodyne technique so that frequency mixing of the two microwave fields occurs [25]. This approach can be applied over a wide frequency range of 0–20 GHz. However, when the microwave frequency was detuned, the system's response changed from a sensitive linear response to an insensitive nonlinear response. Owing to the limitations of the nonresonant second-order Stark effect, the sensitivity at detuning is 20 dB lower than that at resonance, and the sensitivity in the nonresonant region is much smaller than that at the resonant region. Recently, Hu *et al.* improved the measurement sensitivity by applying a strong far-off-resonant local field to generate a Stark shift in the Rydberg atomic energy level and achieved broadband measurement from 0 to 5 GHz using a single Rydberg state [33]. This method requires a suitable Rydberg level to be selected and the laser frequency to be varied when measuring the intensity of the microwave electric field at different frequencies. By adding a local field that resonates with the Rydberg transition, Yao *et al.* used the far-detuned sub-GHz signal field to shift the AT splitting peak generated by the local field [34]. Compared to the conventional AC Stark shift measurement method in this frequency

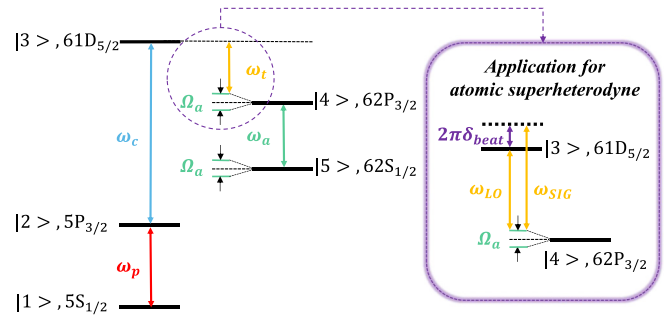


FIG. 1. Five-level scheme of Rydberg EIT-AT splitting with auxiliary microwave dressed. The detailed energy level diagram in the purple frame is the specific scheme applied to the atomic superheterodyne experiment.

band, the sensitivity increased by up to 29 times. However, this highly sensitive measurement technique requires stringent selection of the Rydberg energy level and is only applicable to sub-GHz far-detuned fields. For reference with microwave field regulation, Berweger *et al.* reviewed various schemes for microwave field to regulate the Rydberg energy level and state the advantages of microwave field to tune the Rydberg energy level [35]. The limitations of these previous studies show that a widely applicable and easily implemented measurement method for MW fields across continuous frequency ranges is urgently required.

Based on our previous work [31] and Simons' work [32] on the use of an auxiliary microwave electric field to regulate the Rydberg energy level, we designed and realized a regulation scheme to reconstruct the linear measurement of a detuned field using an auxiliary microwave. The sensitivity of the detuned field measurement was improved by 10 times at most, basically approaching the sensitivity at resonance. The auxiliary field is independent of the energy levels that cause EIT, indicating that the EIT laser frequencies are fixed.

The remainder of this paper is organized as follows. In Sec. II we theoretically study the effects of the auxiliary microwave electric field on the EIT-AT splitting spectrum. We introduce the experimental system and methods in Sec. III. In Sec. IV we investigate the effects of the auxiliary microwave electric field on the EIT-AT splitting spectrum and its regulation on the Rydberg level. Subsequently, we demonstrate the application of this method to atomic superheterodyne measurements to improve the measurement sensitivity of detuning fields. Finally, we provide a summary in Sec. V.

II. THEORETICAL MODEL

We consider a five-level model, as shown in Fig. 1 where $|3\rangle$, $|4\rangle$, and $|5\rangle$ are the Rydberg levels with large principal quantum numbers n . The EIT quantum interference effect is achieved by utilizing the energy-level transition from $|1\rangle$ to $|2\rangle$, which resonates with the frequency ω_p of the probe light, and that from $|2\rangle$ to $|3\rangle$, which resonates with the frequency ω_c of the coupling light. Additionally, a target microwave field is applied, which has a frequency ω_t and resonates with the energy-level transition from $|4\rangle$ to $|3\rangle$. When the amplitude of the target microwave field E_t is sufficiently strong, symmetric

AT splitting is observed based on the EIT spectral signal. The interval of the EIT-AT splitting Δf_i is positively correlated with the Rabi frequency of the target microwave field Ω_t . Considering the Doppler effect at room temperature, the Rabi frequency is given by $\Omega_t = D\Delta f_i$, where D is the residual Doppler parameter. $D = 1$ and $D = \lambda_p/\lambda_c$ correspond to the scanning frequencies of the coupling and probe lights, respectively. E_t and Ω_t are linearly related by $|E_t| = \frac{\hbar}{d_t}\Omega_t$, where \hbar is the reduced Planck's constant, and d_t is the dipole moment of the target microwave atomic transition.

The linear relationship [27,36] between Δf_i and E_t is given by

$$|E_t| = \frac{\hbar}{d_t}\Omega_t = \frac{\hbar}{d_t}D\Delta f_i. \quad (1)$$

The target microwave electric field intensity is traditionally measured through EIT-AT splitting at the target microwave resonance, where the magnitude of the EIT-AT splitting is given by $\Delta f_i = \Omega_t/D$. The interval between the two EIT-AT splitting peaks increased with target microwave detuning. The interval of the EIT-AT splitting Δf_δ with the target microwave

detuning Δ_t [37] is given by

$$\Delta f_\delta = \sqrt{(\Delta_t)^2 + \left(\frac{d_t}{D\hbar}E_t\right)^2}. \quad (2)$$

In this case, the detuning increases, the height of the two EIT-AT splitting peaks becomes more asymmetric until the weak peak becomes indiscernible, which limits the application of EIT-AT splitting in large detuning. It can also be observed from Eq. (2), Δf_δ and E_t no longer exhibit a linear relationship.

An auxiliary microwave field with angular frequency ω_a coupled with levels |5) to |4) is applied to regulate the level |4) such that the resonance is restored between the target microwave field and the dressed Rydberg energy-level transition (Fig. 1). We constructed a five-level model using the Atomic Density Matrix package [38–41] to study the regulation of detuned energy levels using an auxiliary microwave field. The system Hamiltonian under the rotating-wave approximation can be expressed as

$$H = \frac{\hbar}{2} \begin{bmatrix} 0 & \Omega_p & 0 & 0 & 0 \\ \Omega_p & -2\Delta_p & \Omega_c & 0 & 0 \\ 0 & \Omega_c & -2(\Delta_p + \Delta_c) & \Omega_t & \Omega_{2 \times MW} \\ 0 & 0 & \Omega_t & -2(\Delta_p + \Delta_c - \Delta_t) & \Omega_a \\ 0 & 0 & \Omega_{2 \times MW} & \Omega_a & -2(\Delta_p + \Delta_c - \Delta_t - \Delta_a) \end{bmatrix}, \quad (3)$$

where Ω_i and ω_i are the Rabi frequency and frequency of the i th optical field, respectively; $\Delta_i \equiv \omega_i - \omega_{i0}$ is the detuning; and ω_{i0} is the frequency of the atomic-level resonance transition. Subscript i indicates the optical field, where $i = p$ denotes the probe light, $i = c$ denotes the coupling light, $i = t$ denotes the target microwave electric field, and $i = a$ denotes the auxiliary microwave electric field. The effects of the two-photon transition are introduced using the perturbation method [42], where the two-photon Rabi frequency is approximated as $\Omega_{2 \times MW} \propto \Omega_1\Omega_2/2\Delta$, where Ω_1 and Ω_2 are the single-photon Rabi frequencies, and Δ is the detuning of the microwave frequency from the intermediate state [42]. In our model, the detuning of the two microwave fields is dependent on the dressed effect of the other microwave fields on the atomic energy level; that is, $\Delta = \frac{\Omega_a}{2} + \frac{\Omega_t}{2}$. The fitting parameter s is used to characterize the two-photon Rabi frequency $\Omega_{2 \times MW} = s \frac{\Omega_a\Omega_t}{\Omega_a + \Omega_t}$ [31,42], which can be obtained through theoretical calculation or fitting by experimental data; here the s parameter was determined by experimental data fitting and then calculated the data shown in Fig. 2.

The expression for the density matrix element ρ_{21} was obtained from the Hamiltonian in Eq. (3). The detected light transmittance $T = \exp(-\frac{2\pi l}{\lambda_p} \text{Im}[\Xi])$ was then used for the numerical calculations. Here $\Xi = \frac{2N_0}{E_p\epsilon_0} \rho_{21D}$ is the susceptibility, where N_0 is the atomic number density and ρ_{21D} is the Doppler average of the density matrix element ρ_{21} .

Figure 2 shows the numerical simulation results for the regulation effect of the auxiliary microwave field at a

target microwave field detuning of $\Delta_t = 2\pi \times 10$ MHz. The optical field parameters used for the calculation were set to $\Omega_p = 2\pi \times 0.4$ MHz and $\Omega_c = 2\pi \times 3.5$ MHz, similar in magnitude to their values in typical experiments. s was set to 0.01 to model the effect of two-photon transitions. Figure 2(a) shows the evolution of the EIT-AT splitting in the detuned target microwave field as the Rabi frequency of the auxiliary microwave field is varied. As the Rabi frequency of the auxiliary microwave field Ω_a gradually increased from 0 MHz to $2\pi \times 21.3$ MHz, the initial asymmetrical splitting of the two AT peaks became increasingly symmetrical. The splitting is perfectly symmetrical at $\Omega_a = 2\pi \times 21.3$ MHz, at which the detuned target microwave field is again resonant with the target Rydberg level transition. Further increases in Ω_a causes the splitting of the two AT peaks to become asymmetrical in the opposite direction.

A more detailed comparison is shown in Fig. 2(b), in which the EIT without the microwave field, EIT-AT splitting before and after target microwave field detuning, and EIT-AT splitting with symmetry restored under the regulation of the auxiliary microwave field are plotted together. The black solid curve is the EIT signal generated by the system when no microwave field exists, and the red dotted curve is the EIT-AT splitting signal generated by a target microwave field with resonant frequency. The blue dotted curve is the EIT-AT splitting signal generated by a target microwave field with a detuning of $\Delta_t = 2\pi \times 10$ MHz. The two AT splitting peaks in this curve are asymmetrical because of the nonresonant frequency. The purple dotted curve shows that adding an

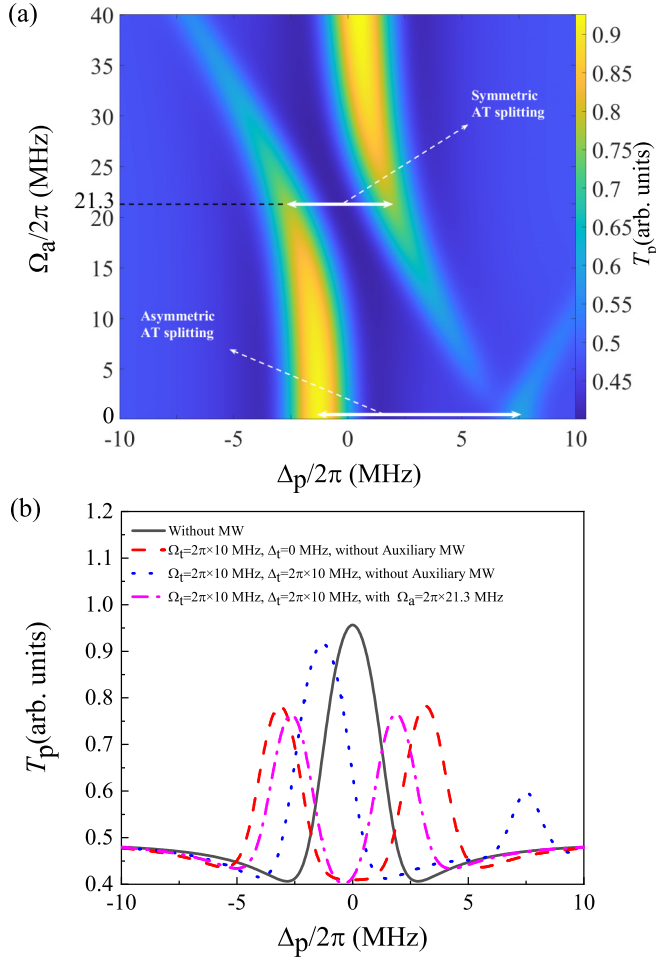


FIG. 2. Spectral images of theoretical numerical calculation. (a) When the detuning of the target microwave field is $\Delta_t = 2\pi \times 10$ MHz and the detuning of the auxiliary field is $\Delta_a = 0$ MHz, spectral regulating effect of different auxiliary microwave electric field Rabi frequency Ω_a . The EIT-AT splitting is symmetric again when $\Omega_a = 2\pi \times 21.3$ MHz. (b) EIT-AT splitting spectral images of theoretical numerical calculation before and after auxiliary microwave electric field dressed.

auxiliary microwave field with $\Omega_a = 2\pi \times 21.3$ MHz provides the most optimal regulation of the target energy level, and the two AT splitting peaks become symmetrical. This implies that the target microwave field, after detuning, is again resonant with the target Rydberg-level transition frequency after the target Rydberg level is dressed by the auxiliary microwave field.

As shown in Fig. 2(b), the EIT-AT splitting interval at this resonance is smaller than the initial resonance. This effect can be explained by the relationship in Eq. (1). Energy level |4> produces two new lines with a spacing width of Ω_a after it is dressed by the auxiliary field. For both positive and negative detuning of the target microwave field, the transition from one of these two lines to level |4> can resonate with the target microwave field again by changing Ω_a . The squared modulus of d_t is proportional to transition probability. Because the transition probability is partially shifted by the presence of the other new line, d_t of the new resonance is smaller than

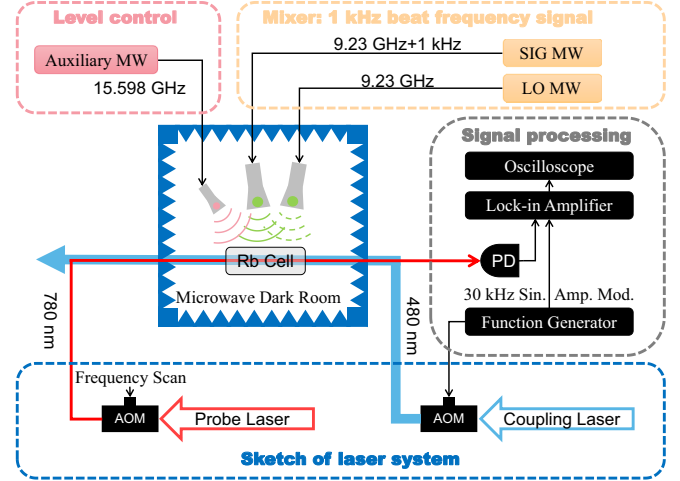


FIG. 3. Experimental setup of Rydberg energy level regulation using an auxiliary microwave.

that of the initial resonance. Conversely, because the intensity $|E_t|$ of the target microwave to be measured and the Doppler parameter D remains unchanged, the reduction in d_t leads to a corresponding reduction in Ω_t and Δf_t .

III. EXPERIMENTAL SETUP AND METHODS

We performed an experiment with an ^{87}Rb vapor cell at room temperature to demonstrate the regulation of the target energy level by an auxiliary field. In the experiment, the $5S_{1/2}(F=2)$, $5P_{3/2}(F=3)$, $61D_{5/2}(F=4)$, $62P_{3/2}(F=3)$, and $62S_{1/2}(F=2)$ levels of ^{87}Rb were used as |1>, |2>, |3>, |4>, and |5> levels of the theoretical model, respectively. Figure 3 shows the experimental setup.

A. Laser system

We used a tunable external-cavity semiconductor laser (DL100, Toptica) to generate the probe light ($\lambda \sim 780$ nm) and a frequency-doubled semiconductor laser (TA-SHG-Pro, Toptica) to generate the coupling light ($\lambda \sim 480$ nm). The two laser beams were fired from opposite directions in the ^{87}Rb vapor cell. The diameters of the probe and coupling lights are approximately $800 \mu\text{m}$ and $900 \mu\text{m}$, respectively, and their light powers $\sim 60 \mu\text{W}$ and 40mW , respectively. The probe light excited the atoms from $5S_{1/2}(F=2)$ to $5P_{3/2}(F=3)$. An acousto-optic modulator (AOM) was used to scan the frequency across a range of ± 25 MHz around the resonant transition frequency within 250 ms. The coupling light excited the atoms from $5P_{3/2}(F=3)$ to $61D_{5/2}(F=4)$ and the laser frequency was locked to the resonant frequency of the transition through Zeeman modulation [39].

B. Signal processing

The intensity of the coupling light was modulated by a 30 kHz sine signal for lock-in detection to improve the signal-to-noise ratio of the EIT-AT spectra [40]. After the probe light interacted with the coupling light, microwaves, and atoms in the ^{87}Rb vapor cell, a photodetector (PDA36A2, Thorlabs)

recorded the probe light intensity and sent it to a lock-in amplifier (LI5640, NF Corporation).

C. Mixer

Two signal sources (E8257D, Keysight Technologies; 8340B, HP Corporation) were connected to two horn antennas in the microwave dark room to generate microwave electric fields at the resonance frequency (~ 9.23 GHz) of the $62P_{3/2}(F=3)$ to $61D_{5/2}(F=4)$ Rydberg transition as the signal and local fields in the experiment, respectively. Only the signal source of the LO field was turned on in the EIT-AT splitting experiment. Meanwhile, in the nonresonant heterodyne mixing experiment, we further opened the SIG field to form a beat signal. An appropriate beat signal with a frequency of 1 kHz was generated by adjusting the intensity of the two microwave fields.

The response of the Rydberg sensor to MW frequency can be intuitively explained as follows [25]. The Stark shift of the target Rydberg state takes the linear form of AT splitting in the near-resonance region as follows:

$$\Omega_{\text{on res}} = |E_t|d_t/\hbar. \quad (4)$$

In the far-detuned region away from resonance, the Stark shift is induced by a weak nonlinear effect,

$$\Omega_{\text{off res}} = -\frac{1}{2}\alpha|E_t|^2, \quad (5)$$

where α denotes atomic polarizability.

The signal field is given by $E_{\text{SIG}} \cos[(\omega + \delta_{\text{beat}})t]$, and the LO field is given by $E_{\text{LO}} \cos(\omega t - \phi_{\text{LO}})$. Assuming that $\omega \gg \delta_{\text{beat}}$ and ω are less than the instantaneous bandwidth, the detected light intensity is reflected in the total field. Away from resonance, the total field can be approximated using a nonlinear relation [25,43]:

$$T_{\text{probe}} \propto \langle E_{\text{tot}} \rangle_{\tau} \approx \left[(E_{\text{SIG}}^2 + E_{\text{LO}}^2) / 2 + E_{\text{SIG}} E_{\text{LO}} \cos(\delta_{\text{beat}} t + \phi_{\text{LO}}) \right]^{1/2}. \quad (6)$$

In the near-resonance case, which is the AT regime, the following approximate linear relationship holds when $E_{\text{LO}} \gg E_{\text{SIG}}$ [25,43]:

$$T_{\text{probe}} \propto \langle E_{\text{tot}} \rangle_{\tau} \approx \frac{E_{\text{LO}}}{2} + \frac{E_{\text{SIG}}}{2} \cos(\delta_{\text{beat}} t + \phi_{\text{LO}}). \quad (7)$$

D. Level regulation

We connected a horn antenna in a microwave dark room to a third signal source (8340 B, HP Corporation) and generated a microwave electric field corresponding to the resonant frequency (~ 15.598 GHz) of the $62S_{1/2}(F=2)$ to $62P_{3/2}(F=3)$ Rydberg transition as an auxiliary field for energy level regulation. By changing the output power of the microwave source and subsequently the Rabi frequency of the auxiliary field, the target energy level was correspondingly regulated.

IV. RESULTS AND DISCUSSION

A. EIT-AT splitting experiment results

We first discuss the experimental results for the modification of the EIT-AT splitting spectra using an auxiliary

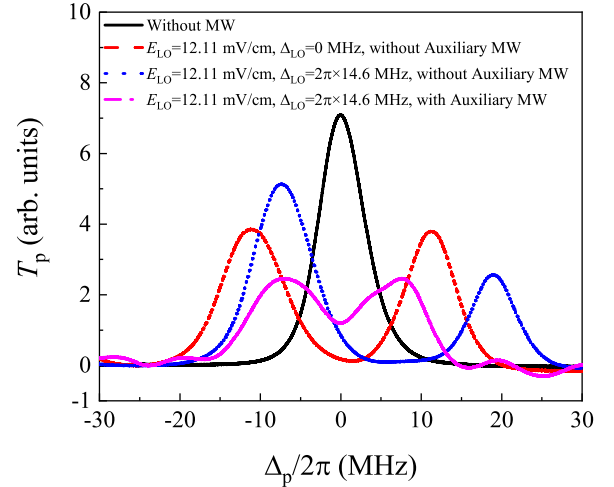


FIG. 4. Spectral images of EIT-AT splitting experiment before and after auxiliary microwave electric field dressed. Black solid curve: EIT signal generated by the system when there is no microwave field. Red dotted curve: symmetrical EIT-AT splitting at resonance. Blue dotted curve: asymmetric EIT-AT splitting at detuning $\Delta_{\text{LO}} = 2\pi \times 14.6$ MHz. Purple dotted curve: the again symmetrical EIT-AT splitting after auxiliary field dressed. The EIT-AT splitting is again symmetrical. This indicates that the detuned local microwave field and the target Rydberg-level transition frequency dressed by the auxiliary microwave field is resonated again. Experimental parameters of lock-in amplifier: sensitivity 5 mV, time constant 1 ms.

microwave field. Figure 4 shows the signal spectra generated by the local microwave field in the EIT-AT splitting spectrum experiment before and after the application of the auxiliary microwave electric field. The black solid curve represents the basic EIT spectral signal generated by the system without a microwave field. When the local microwave field frequency is resonant with the transition frequency, the detuning $\Delta_{\text{LO}} = 2\pi \times (f_{\text{LO}} - f_0) = 0$ MHz, which corresponds to $f_{\text{LO}} \cong f_0 = 9.2328$ GHz, and the original single EIT peak split and forms two symmetrical EIT-AT splitting peaks, as shown by the red dotted curve in Fig. 4. When the frequency of the local microwave field was detuned to $\Delta_{\text{LO}} = 2\pi \times (f_{\text{LO}} - f_0) = 2\pi \times 14.6$ MHz, the microwave frequency was nonresonant, and the heights of the two EIT-AT splitting peaks were asymmetric, as shown by the blue dotted curve in Fig. 4. After applying an auxiliary microwave field resonant with the transition frequency $f'_0 = 15.598$ GHz of the $|4\rangle$ and $|5\rangle$ Rydberg levels in the energy-level model shown in Fig. 1, the heights of the two EIT-AT splitting peaks were symmetrical again, as shown by the purple dotted curve in Fig. 4. This means that the detuned local microwave field was again resonant with the target Rydberg-level transition frequency after the latter was dressed by the auxiliary microwave field. Additionally, the system's response to the Rabi frequency of the microwave field changed from the original nonresonant second-order nonlinear effect to the first-order linear effect.

The results show that the spectral data are very smooth when there is no microwave field or applied only one microwave field. When we applied both microwave fields to the system, there was a weak oscillation in the EIT-AT spectra

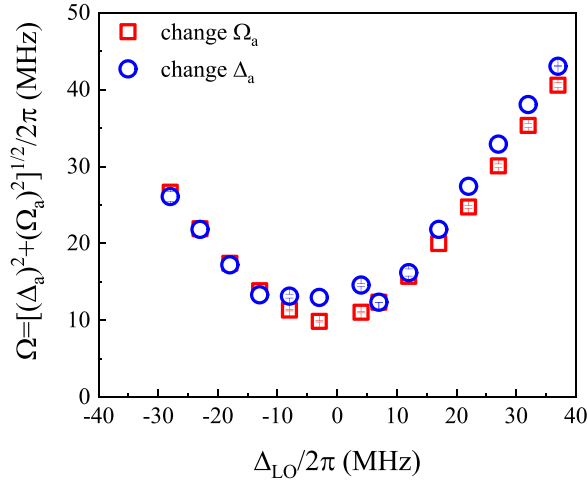


FIG. 5. The best matching curve of the generalized Rabi frequency of the auxiliary microwave field to the local microwave field detuning. Red square dotted line: The demand degree relation of generalized Rabi frequency Ω for achieving the best response effect of Rydberg energy level by changing Rabi frequency Ω_a of auxiliary field. Blue circle dotted line: The demand degree relation of generalized Rabi frequency Ω for achieving the best response effect of Rydberg energy level by changing detuning Δ_a of auxiliary field. Their generally consistent trend degree reflects their equivalence. The demand degree refers to the extent to which we need the Ω_a or Δ_a to achieve the best regulation effect.

(pink curve in Fig. 4). These oscillations were caused by the combination of the auxiliary microwave field (~ 15.6 GHz) and local field (~ 9.2 GHz). Because the amplitudes of these oscillations are far smaller than the intensity of the EIT-AT spectra we are interested in, and its phase is stable, it will not affect our experimental results and analysis.

The visible difference between the magnitudes of the EIT-AT splitting in the red and purple curves implies that the linear relationship of the Rabi frequency response of the system also changed because of the change in the transition dipole moment d_{MW} . This result was consistent with the theoretical predictions presented in Sec. II.

B. Regulation effect of the auxiliary field

Next, we discuss the regulating effect of the power and frequency of the auxiliary microwave electric field at the target Rydberg level. The experimental results are shown in Fig. 5. By varying the output power of the microwave source for the auxiliary field to change the Rabi frequency Ω_a or varying the auxiliary field detuning $\Delta_a = 2\pi \times (f_a - f'_0)$, the generalized Rabi frequency can be set to $\Omega = \sqrt{\Delta_a^2 + \Omega_a^2}$ [31,37]. For each given value of the local microwave field detuning Δ_{LO} , there is a best-matching combination of the Ω_a and Δ_a parameters for the auxiliary field that causes the detuned local microwave field to become resonant. For experimental and application convenience, we change one of Ω_a or Δ_a separately to achieve the best match.

Δ_a was first set to a fixed value of 0 MHz. The resultant generalized Rabi frequency Ω corresponding to the best-matching Rabi frequency Ω_a was plotted as a function of Δ_{LO}

in the red square dotted line in Fig. 5. This line intuitively shows the Rabi frequency of the auxiliary field required to achieve the best regulating effect for the Rydberg energy level. Similarly, the output power of the microwave source was fixed at 5 dBm, which was equivalent to a fixed Rabi frequency of $\Omega_a = 2\pi \times 12.4502$ MHz. The generalized Rabi frequency Ω corresponding to the best-matching auxiliary field detuning Δ_a is plotted against Δ_{LO} in a line composed of blue circles in Fig. 5. A comparison of the curves obtained by varying the two parameters Ω_a and Δ_a indicates that the Rydberg level can be equivalently regulated through either the strength or frequency of the auxiliary microwave field.

The larger the detuning Δ_{LO} of the local microwave field, the better the effect of changing the Rabi frequency Ω_a of the auxiliary microwave than that of changing the detuning Δ_a . This is because, as the detuning of the auxiliary microwave field increased, the height of the EIT-AT splitting bimodal became more asymmetrical. That is, changing Δ_a reduced the population of dressed energy level states far away from the resonance level. Therefore, the spectral peak intensity was far from the resonance center, as shown in the right EIT-AT splitting peak on the blue curve in Fig. 4. Hence, we set Ω_a to the resonant frequency $f'_0 = 15.598$ GHz and regulated the Rydberg energy level by changing Ω_a . The maximum detuning range of the controllable local microwave field in this approach was limited by the maximum output power of the microwave source for the auxiliary field.

C. Nonresonant heterodyne mixing experiment

Based on the above results, we combined the energy-level regulation method with the atomic heterodyne technique to improve the measurement sensitivity for detuned microwave electric fields and further demonstrate the feasibility of this scheme. We used a mixer to obtain a beat signal of $\delta_{\text{beat}} = 2\pi \times (f_{\text{SIG}} - f_{\text{LO}}) = 2\pi \times 1$ kHz for atomic heterodyne measurements of the microwave electric field. The frequency difference between the signal and local microwave fields of the beat signal formed by the mixer was 1 kHz, which is much smaller than the frequency magnitude of the detuning. Therefore, the detuning of the signal field could be approximated as Δ_{LO} in the experiment to use the beat signal to characterize the response to the microwave field signal.

When the signal field was resonant, the beat signal amplitude was at its maximum, as indicated by the black solid line in Fig. 6. The red dotted line in Fig. 6 shows a specific example of frequency detuning of $\Delta_{LO} = -2\pi \times 16$ MHz. Compared with the beat signal amplitude of 2.443 V at the resonance point, the beat signal amplitude at the $-2\pi \times 16$ MHz detuning point was 0.277 V. Therefore, the beat amplitude at the resonance point is approximately 8.82 times that at the $-2\pi \times 16$ MHz detuning point. An auxiliary field with a frequency of $f_a = f'_0 = 15.598$ GHz was subsequently added, and the output power of the microwave source was adjusted to -11 dBm to achieve the best match, as discussed in Sec. IV B. As shown by the blue dotted line in Fig. 6, the beat signal amplitude under the action of the auxiliary field significantly increased to 0.883 V, which is 3.2 times that of the amplitude under detuning and without the auxiliary field.

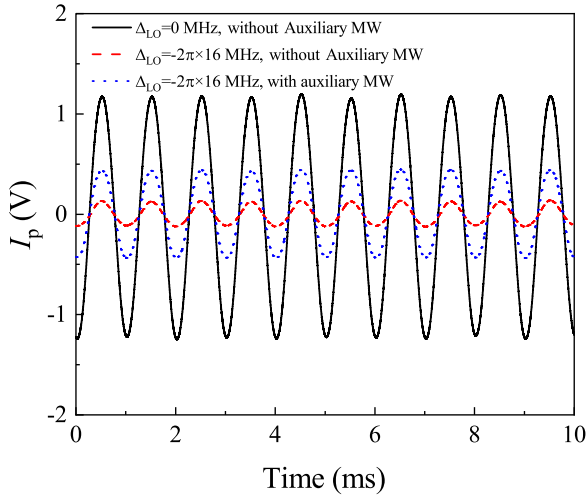


FIG. 6. The influence of auxiliary microwave electric field on beat signal under heterodyne method. The black solid line is the beat signal of the resonance point, the red dotted line is the beat signal of the $\Delta_{LO} = -2\pi \times 16$ MHz detuning point, and the blue dotted line is the beat signal after the intervention of the best matched auxiliary field of the $\Delta_{LO} = -2\pi \times 16$ MHz detuning point. The beat amplitude is significantly enhanced after the auxiliary field intervention, and the response of the beat amplitude to the microwave field strength returns to the most sensitive linear effect in resonance. Experimental parameters of lock-in amplifier: sensitivity 2 mV, time constant 100 μ s.

Based on this, we conducted an experimental study on the effect of the auxiliary microwave field on the beat signal amplitude within the detuning frequency range of $\Delta_{LO}/2\pi = -100$ –0 MHz. Figure 7 shows the detailed measurement results, in which the beat signal amplitudes with and without the auxiliary field are plotted against Δ_{LO} . The lower panel of Fig. 7 shows corresponding optimal matching Ω_a , the maximum Ω_a is limited by the maximum output power 13.5 dBm of our microwave source. The amplitudes of the beat signal were obtained based on the existing 1 kHz beat signal and by gradually increasing the detuning in the negative direction starting from the resonance point of $\Delta_{LO}/2\pi = 0$ MHz until $\Delta_{LO}/2\pi = -100$ MHz. These signals are shown by the line composed of black squares in Fig. 7, which provides an intuitive reflection of the beat signal amplitude response to the detuning $\Delta_{LO}/2\pi$ in the conventional nonresonant heterodyne method within a detuning frequency range of -100 –0 MHz. The beat signal amplitude was the largest at resonance, decreased rapidly as the detuning Δ_{LO} increased in the negative direction, and reached its minimum value at approximately $-2\pi \times 16$ MHz before rising slowly. The slowly rising stage may be attributed to $61D_{3/2}$, $62P_{1/2}$, or other similar Rydberg levels.

After the auxiliary microwave field was applied, the best-matching Rabi frequency for regulating the Rydberg energy level was set at each detuning point. The corresponding beat amplitudes are indicated by red dotted circles in Fig. 7. The results intuitively reflect the response of the beat signal amplitude to the detuning amount across the frequency detuning range of -100 –0 MHz in the nonresonant heterodyne method

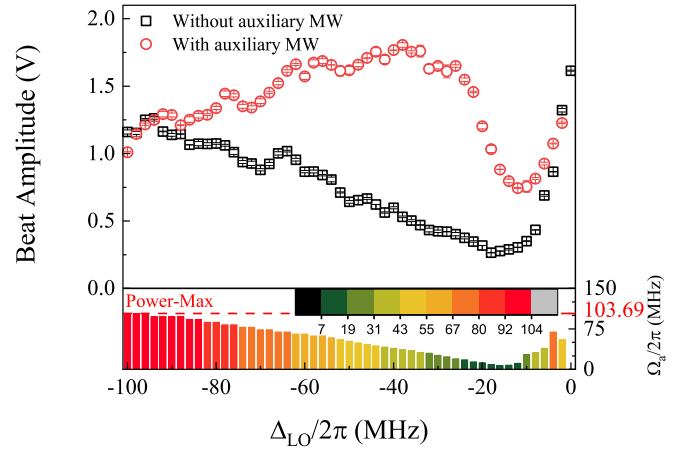


FIG. 7. Response curve of beat frequency signal amplitude before and after auxiliary microwave field intervention under nonresonant heterodyne method within the frequency detuning range from 0 to -100 MHz. Black square dotted line: the response relationship between the beat signal amplitude of the ordinary nonresonant heterodyne method and the detuning $\Delta_{LO}/2\pi$. Red circle dotted line: the response relationship between the amplitude of nonresonant heterodyne beat signal and the detuning $\Delta_{LO}/2\pi$ under the intervention of auxiliary field. The intervention of auxiliary field provides a wide and high-sensitivity linear response frequency range of 100 MHz. Lower panel: the height of histogram and color bar correspond to optimal matching auxiliary field Rabi frequency and mark the upper limit of our microwave source power with “Power-Max.” Experimental parameters of lock-in amplifier: sensitivity 5 mV, time constant 100 μ s.

under the intervention of the auxiliary field. The beat signal amplitude was significantly improved compared with that without auxiliary field intervention. At the detuning point of $\Delta_{LO} = -2\pi \times 22$ MHz, the amplitude of the beat signal was increased by 4.3 times through the intervention of the auxiliary field. By comparing the lines composed of black squares and red circles in Fig. 7, the auxiliary field not only transformed the nonresonant effect of detuning into a resonant effect in the frequency detuning range of -100 –0 MHz but also significantly improved the broadband measurement sensitivity of the detuned point. That is, the width of the detuning interval from 0 to -100 MHz can completely cover the effective interval for the nonlinear response of a single $62P_{3/2}$ Rydberg energy level, which is highly significant for filling the potential nonlinear response interval between hundreds of Rydberg energy levels that are greater than 100 MHz and far from resonance. The width of this effective detuning interval is larger if no interference from $61D_{3/2}$, $62P_{1/2}$, or other similar Rydberg levels occurs.

D. Analysis of sensitivity enhancement

We now discuss the effect of the auxiliary microwave field on the beat amplitude in atomic superheterodyne measurements, and the minimum measurable value at a given detuning point. Figure 8 shows the measurement results for the ordinary heterodyne method with detuning Δ_{LO} of 0 MHz and $-2\pi \times 22$ MHz and the results for auxiliary field intervention with a detuning Δ_{LO} of $-2\pi \times 22$ MHz. The line comprising black squares corresponds to the $\Delta_{LO} = 0$ MHz resonance

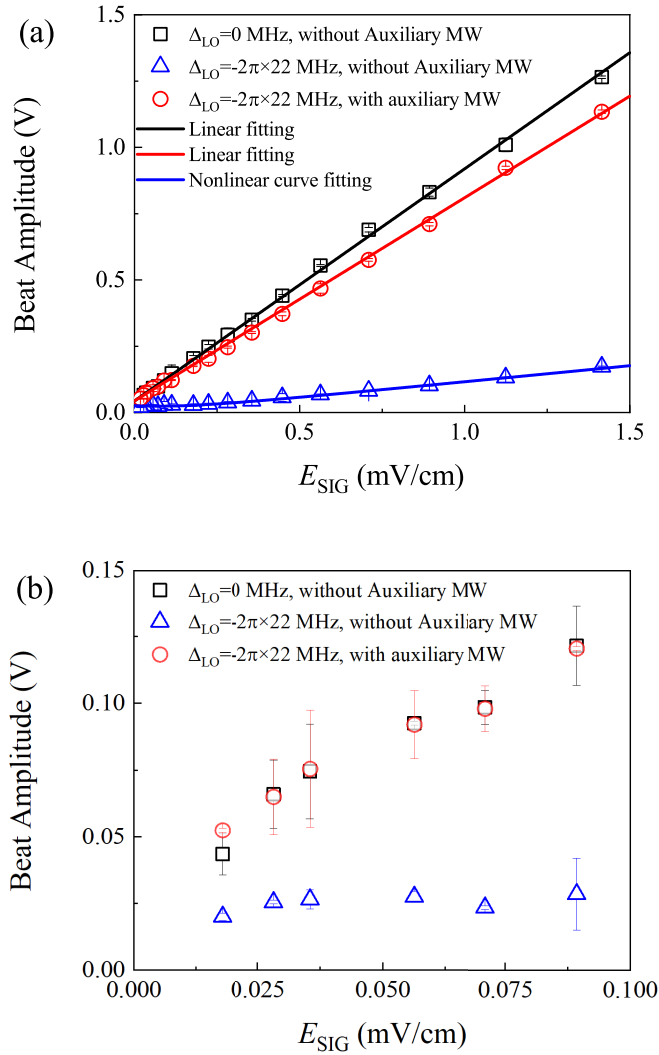


FIG. 8. The relationship between the beat signal amplitude and the microwave electric field strength to be measured at the resonance point of $\Delta_{\text{LO}} = 0$ MHz and the detuning point of $\Delta_{\text{LO}} = -2\pi \times 22$ MHz by the heterodyne method before and after the auxiliary microwave field intervention. Black square dotted line: at the resonance point, the minimum measurable value is $18 \mu\text{V}/\text{cm}$. Blue triangle dot line: at the detuning point, the minimum measurable value is $180 \mu\text{V}/\text{cm}$. Red circle dotted line: at the detuning point, with the auxiliary microwave field intervention, the minimum measurable value is $18 \mu\text{V}/\text{cm}$. The heterodyne method of auxiliary field intervention can basically reach the measurement limit value at resonance. Panel (b) is a detailed drawing within the scope of panel (a) $E_{\text{SIG}} \leq 0.1$ mV/cm. Experimental parameters of lock-in amplifier: sensitivity 2 mV, time constant 100 μs .

point. The amplitude of the beat signal varied linearly with the microwave electric field strength and was measured within the field strength range of 0-1.5 mV/cm. The solid black line represents a linear fit based on Eq. (7). This is consistent with results reported in the literature [43,44]. In our setup, the minimum electric-field intensity that could be measured at the resonance point using the ordinary atom heterodyne method was $18 \mu\text{V}/\text{cm}$. The blue triangles correspond to the $\Delta_{\text{LO}} = -2\pi \times 22$ MHz detuning point, where the beat signal

varied with the microwave electric field strength to be measured, and the minimum measurable electric field strength was $180 \mu\text{V}/\text{cm}$. The solid blue line is a nonlinear curve fit obtained based on Eq. (6). The line composed of red circles corresponds to the $\Delta_{\text{LO}} = -2\pi \times 22$ MHz detuning point under the intervention of the best matching auxiliary field. From the corresponding linear fit shown by the red solid line, it can be observed that the amplitude of the beat signal retained a good linear relationship with the electric field strength, and the minimum measured value reached $18 \mu\text{V}/\text{cm}$. This value is the measurement limit at resonance. It is 10 times higher than the minimum measurement limit of the ordinary heterodyne method at the $\Delta_{\text{LO}} = -2\pi \times 22$ MHz detuning point. From the fitting results in Fig. 8(a), we can see the linear and nonlinear relationship between beat amplitude and E_{SIG} . When $\Delta_{\text{LO}} = 0$ MHz, the beat amplitude has a good linear relationship with E_{SIG} , as shown by the black solid line in Fig. 8(a). When it becomes nonresonant, the beat amplitude has a nonlinear relationship with E_{SIG} , as shown by blue solid line in Fig. 8(a). At this time, the beat amplitude is insensitive to E_{SIG} , which is not conducive to the measurement of E_{SIG} . Interestingly, under the effect of the auxiliary microwave electric field, the nonresonance relationship at the time of detuning becomes linear again, as shown in the red circle dotted line in Fig. 8(a). Therefore, the nonlinear response of the mixer to the microwave field strength of the detuned target will become a linear response with the addition of auxiliary field. The results indicate that the auxiliary microwave field not only retained a linear relationship between the amplitude of the beat signal and the electric field strength but also improved the measurement sensitivity, which could approximately reach that at the resonance point.

Finally, we examined the improvement in the measurement sensitivity at the best-matching auxiliary microwave Rabi frequency in the frequency detuning range of -100 – 0 MHz. Figure 9 shows the results of the minimum measurement limit with and without an auxiliary microwave electric field. The line composed of black squares shows the relationship between the minimum measurement limit and detuning $\Delta_{\text{LO}}/2\pi$ without the intervention of the auxiliary field. The line composed of red circles shows the relationship between the minimum measurement limit and detuning $\Delta_{\text{LO}}/2\pi$ under optimal auxiliary field intervention. Across the entire detuning range, the intervention of the auxiliary field resulted in better measurement sensitivity, which was reflected in the smaller measurement limit. The lower panel of Fig. 9 shows corresponding optimal matching Ω_a , the maximum Ω_a is limited by the maximum output power 13.5 dBm of our microwave source. Therefore, from the experimental results, the auxiliary field resulted in a significantly improved measurement sensitivity of up to 20 dB in the frequency detuning range of 0 to -100 MHz. Because the electric field strength is proportional to the arithmetic square root of the power, the measurement sensitivity improved by a factor of approximately 10. The results indicate that our method can increase the linear response interval of Rydberg-level transitions by at least 100 MHz. This essentially covers the energy-level intervals of typical hyperfine structures and achieves a higher measurement sensitivity in the extended linear response interval.

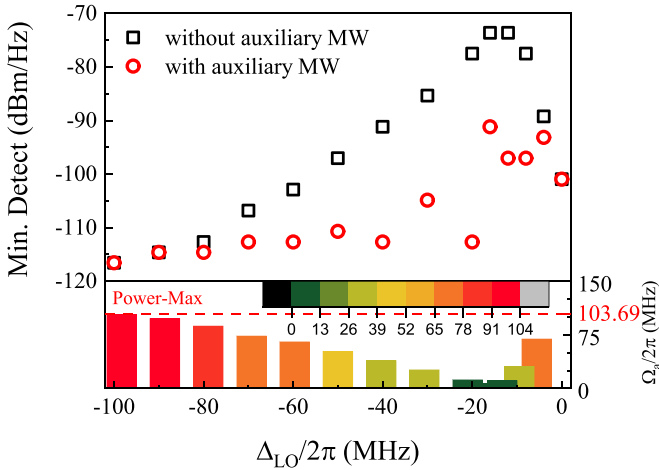


FIG. 9. Comparison diagram of measurement sensitivity with and without auxiliary microwave electric field in the frequency detuning range from 0 to -100 MHz. Black square dotted line: the relationship curve between the minimum measurement limit and the detuning $\Delta_{LO}/2\pi$ without the intervention of auxiliary field. Red circle dot line: the curve of the relationship between the minimum measurement limit and the detuning $\Delta_{LO}/2\pi$ under the optimal matching auxiliary field intervention. The lower panel: the height of histogram and color bar correspond to optimal matching auxiliary field Rabi frequency, and mark the upper limit of our microwave source power with “Power-Max.” In the experimental detuning interval, the intervention of auxiliary field can basically achieve better measurement sensitivity. Experimental parameters of lock-in amplifier: sensitivity 2 mV, time constant 100 μ s.

The factor of 10 is limited by our modest experimental setup. As shown in Fig. 9, the black square dotted line shows the sensitivity results obtained by the atomic superheterodyne method without the auxiliary microwave field when the target MW field is detuning from 0 to -100 MHz. We can observe that the sensitivity can be improved to a better level within the range of -20 to -100 MHz than that at resonance, similar to a recent article that discussed the enhancement of the sensitivity by detuning the frequency of the local microwave [18]. Interestingly, the sensitivity of the atomic superheterodyne method is improved over the detuning range of -100 – 0 MHz by the auxiliary microwave field, as shown by the red dotted circle in Fig. 9, and better sensitivity can be achieved in the -20 to -100 MHz range than at resonance.

In addition, we have built a simple five-level model for a theoretical explanation to improve the sensitivity when the frequency of the microwave electric field is detuning. Simultaneously, if the Rydberg energy levels are sufficiently dense, the role of multiple energy levels should be considered. However, most of them are in the sensitive resonance region, and good sensitivity can be obtained without using an auxiliary microwave electric field to regulate Rydberg energy levels. Another thing we need to explicate about is the absolute calibration loss of the signal microwave electric field in our scheme. The difficulty is the accurate calculation of the dipole transition matrix elements dressed by the auxiliary

microwave electric field. So even if we know the parameters of the auxiliary field, it is still difficult to reproduce the absolute calibration of the signal field with our method, and absolute calibration is not the aim of this article.

V. CONCLUSION

In summary, we theoretically and experimentally demonstrated the use of an auxiliary microwave field to regulate the target Rydberg energy levels so that resonance is restored between the detuned target microwave field and the Rydberg-Rydberg transition used for sensing. When the target microwave field is detuned, the target Rydberg energy levels can be regulated without affecting other energy levels. This can be achieved by changing the power or detuning of the auxiliary microwave field so that the symmetry of the two AT splitting peaks in the EIT-AT splitting spectrum is restored. Our method can be widely applied to various Rydberg energy levels and is widely applicable for other technologies, which shows advantages in the application for atomic superheterodyne technology. The addition of the auxiliary field can change the nonlinear response of the mixer to the detuned target microwave field strength to a linear response and the maximum beat frequency amplitude occurred when resonance was restored. The maximum measurement sensitivity can be increased by 20 dB, equivalent to an increase in the conventional atomic superheterodyne technology by approximately 10 times. Such high-sensitivity measurements can be realized within a frequency range of 100 MHz. Our method allows the use of auxiliary fields to only regulate the target Rydberg energy levels, which can be implemented without changing the EIT laser frequency and overcome the disadvantages of other external fields affecting all energy levels. A specific auxiliary field parameter can be found to achieve high bandwidth sensitivity measurement as long as the specific energy levels and the detuning of target fields are determined. It has high application value in engineering without changing the laser frequencies during regulation, as confirmed by the experimental results applied to the atomic superheterodyne method.

ACKNOWLEDGMENTS

We are grateful for fruitful discussions with Prof. T. F. Gallagher at the University of Virginia; Dr. Yuechun Jiao, Prof. Linjie Zhang, and Prof. Jie Ma at Shanxi University; Dr. Kaiyu Liao and Prof. Hui Yan at South China Normal University; and Dr. Fei Meng at the National Institute of Metrology, China. This project was supported by the Beijing Natural Science Foundation (Grant No. 1212014), the National Natural Science Foundation of China (Grants No. 11604334, 11604177, and U2031125), the Key Research Program of the Chinese Academy of Sciences (Grant No. XDPB08-3), the Fundamental Research Funds for the Central Universities, the National Key Research and Development Program of China (Grants No. 2017YFA0304900 and 2017YFA0402300), and Youth Innovation Promotion Association CAS. The authors declare no conflicts of interest.

- [1] C. L. Degen, F. Reinhard, and P. Cappellaro, Quantum sensing, *Rev. Mod. Phys.* **89**, 035002 (2017).
- [2] T. Gallagher, Rydberg atoms, in *Springer Handbook of Atomic, Molecular, and Optical Physics*, edited by G. Drake (Springer, New York, 2006), pp. 235–245.
- [3] A. D. Ludlow, M. M. Boyd, J. Ye, E. Peik, and P. O. Schmidt, Optical atomic clocks, *Rev. Mod. Phys.* **87**, 637 (2015).
- [4] N. Huntemann, C. Sanner, B. Lipphardt, C. Tamm, and E. Peik, Single-Ion Atomic Clock with 3×10^{-18} Systematic Uncertainty, *Phys. Rev. Lett.* **116**, 063001 (2016).
- [5] I. K. Kominis, T. W. Kornack, J. C. Allred, and M. V. Romalis, A subfemtotesla multichannel atomic magnetometer, *Nature (London)* **422**, 596 (2003).
- [6] R. Mhaskar, S. Knappe, and J. Kitching, A low-power, high-sensitivity micromachined optical magnetometer, *Appl. Phys. Lett.* **101**, 241105 (2012).
- [7] J. Fang and J. Qin, Advances in atomic gyroscopes: A view from inertial navigation applications, *Sensors* **12**, 6331 (2012).
- [8] L. A. Downes, A. R. MacKellar, D. J. Whiting, C. Bourgenot, C. S. Adams, and K. J. Weatherill, Full-Field Terahertz Imaging at KiloHertz Frame Rates Using Atomic Vapor, *Phys. Rev. X* **10**, 011027 (2020).
- [9] S. Yoshida, C. O. Reinhold, J. Burgdörfer, S. Ye, and F. B. Dunning, Photoexcitation of $n \simeq 305$ Rydberg states in the presence of an rf drive field, *Phys. Rev. A* **86**, 043415 (2012).
- [10] A. Osterwalder and F. Merkt, Using High Rydberg States as Electric Field Sensors, *Phys. Rev. Lett.* **82**, 1831 (1999).
- [11] J. M. Raimond, M. Brune, and S. Haroche, Manipulating quantum entanglement with atoms and photons in a cavity, *Rev. Mod. Phys.* **73**, 565 (2001).
- [12] L.-H. Zhang, Z.-K. Liu, B. Liu, Z.-Y. Zhang, G.-C. Guo, D.-S. Ding, and B.-S. Shi, Rydberg Microwave-Frequency-Comb Spectrometer, *Phys. Rev. Appl.* **18**, 014033 (2022).
- [13] M. Fleischhauer, A. Imamoglu, and J. P. Marangos, Electromagnetically induced transparency: Optics in coherent media, *Rev. Mod. Phys.* **77**, 633 (2005).
- [14] J. Han, T. Vogt, C. Gross, D. Jaksch, M. Kiffner, and W. Li, Coherent Microwave-to-Optical Conversion via Six-Wave Mixing in Rydberg Atoms, *Phys. Rev. Lett.* **120**, 093201 (2018).
- [15] S. D. Hogan, J. A. Agner, F. Merkt, T. Thiele, S. Filipp, and A. Wallraff, Driving Rydberg-Rydberg Transitions from a Coplanar Microwave Waveguide, *Phys. Rev. Lett.* **108**, 063004 (2012).
- [16] A. A. Morgan and S. D. Hogan, Coupling Rydberg Atoms to Microwave Fields in a Superconducting Coplanar Waveguide Resonator, *Phys. Rev. Lett.* **124**, 193604 (2020).
- [17] K. C. Cox, D. H. Meyer, F. K. Fatemi, and P. D. Kunz, Quantum-Limited Atomic Receiver in the Electrically Small Regime, *Phys. Rev. Lett.* **121**, 110502 (2018).
- [18] M. Cai, Z. Xu, S. You, and H. Liu, Sensitivity improvement and determination of Rydberg atom-based microwave sensor, *Photonics* **9**, 250 (2022).
- [19] A. Artusio-Glimpse, M. T. Simons, N. Prajapati, and C. L. Holloway, Modern RF measurements with hot atoms: A technology review of Rydberg atom-based radio frequency field sensors, *IEEE Microw. Mag.* **23**, 44 (2022).
- [20] E. Paradis, G. Raithel, and D. A. Anderson, Atomic measurements of high-intensity VHF-band radio-frequency fields with a Rydberg vapor-cell detector, *Phys. Rev. A* **100**, 013420 (2019).
- [21] K.-Y. Liao, H.-T. Tu, S.-Z. Yang, C.-J. Chen, X.-H. Liu, J. Liang, X.-D. Zhang, H. Yan, and S.-L. Zhu, Microwave electrometry via electromagnetically induced absorption in cold Rydberg atoms, *Phys. Rev. A* **101**, 053432 (2020).
- [22] J. A. Sedlacek, A. Schwettmann, H. Kübler, and J. P. Shaffer, Atom-Based Vector Microwave Electrometry Using Rubidium Rydberg Atoms in a Vapor Cell, *Phys. Rev. Lett.* **111**, 063001 (2013).
- [23] Z. Bai, C. S. Adams, G. Huang, and W. Li, Self-Induced Transparency in Warm and Strongly Interacting Rydberg Gases, *Phys. Rev. Lett.* **125**, 263605 (2020).
- [24] Y.-Y. Jau and T. Carter, Vapor-Cell-Based Atomic Electrometry for Detection Frequencies below 1 kHz, *Phys. Rev. Appl.* **13**, 054034 (2020).
- [25] D. H. Meyer, P. D. Kunz, and K. C. Cox, Waveguide-Coupled Rydberg Spectrum Analyzer from 0 to 20 GHz, *Phys. Rev. Appl.* **15**, 014053 (2021).
- [26] A. K. Mohapatra, T. R. Jackson, and C. S. Adams, Coherent Optical Detection of Highly Excited Rydberg States Using Electromagnetically Induced Transparency, *Phys. Rev. Lett.* **98**, 113003 (2007).
- [27] J. A. Sedlacek, A. Schwettmann, H. Kübler, R. Lw, T. Pfau, and J. P. Shaffer, Microwave electrometry with Rydberg atoms in a vapour cell using bright atomic resonances, *Nat. Phys.* **8**, 819 (2012).
- [28] M. Tanasittikosol, J. D. Pritchard, D. Maxwell, A. Gauguier, K. J. Weatherill, R. M. Potvliege, and C. S. Adams, Microwave dressing of Rydberg dark states, *J. Phys. B: At. Mol. Opt. Phys.* **44**, 184020 (2011).
- [29] L. Zhang, S. Bao, H. Zhang, G. Raithel, J. Zhao, L. Xiao, and S. Jia, Interplay between optical pumping and Rydberg EIT in magnetic fields, *Opt. Express* **26**, 29931 (2018).
- [30] L. Chai and R. Jones, Demonstration of an RF electrometer based on EIT spectroscopy of non-resonantly dressed Rydberg atoms, *Conference on Lasers and Electro-Optics (2021) STu2A.1*.
- [31] F.-D. Jia, X.-B. Liu, J. Mei, Y.-H. Yu, H.-Y. Zhang, Z.-Q. Lin, H.-Y. Dong, J. Zhang, F. Xie, and Z.-P. Zhong, Span shift and extension of quantum microwave electrometry with Rydberg atoms dressed by an auxiliary microwave field, *Phys. Rev. A* **103**, 063113 (2021).
- [32] M. T. Simons, A. B. Artusio-Glimpse, C. L. Holloway, E. Imhof, S. R. Jefferts, R. Wyllie, B. C. Sawyer, and T. G. Walker, Continuous radio-frequency electric-field detection through adjacent Rydberg resonance tuning, *Phys. Rev. A* **104**, 032824 (2021).
- [33] J. Hu, H. Li, R. Song, J. Bai, Y. Jiao, J. Zhao, and S. Jia, Continuously tunable radio frequency electrometry with Rydberg atoms, *Appl. Phys. Lett.* **121**, 014002 (2022).
- [34] J. Yao, Q. An, Y. Zhou, K. Yang, F. Wu, and Y. Fu, Sensitivity enhancement of far-detuned RF field sensing based on Rydberg atoms dressed by a near-resonant RF field, *Opt. Lett.* **47**, 5256 (2022).
- [35] S. Berweger, N. Prajapati, A. B. Artusio-Glimpse, A. P. Rotunno, R. Brown, C. L. Holloway, M. T. Simons, E. Imhof, S. R. Jefferts, B. N. Kayim *et al.*, Rydberg state engineering: A comparison of tuning schemes for continuous frequency sensing, [arXiv:2209.14407](https://arxiv.org/abs/2209.14407).

- [36] H. Fan, S. Kumar, J. Sedlacek, H. Kübler, S. Karimkashi, and J. P. Shaffer, Atom based RF electric field sensing, *J. Phys. B: At. Mol. Opt. Phys.* **48**, 202001 (2015).
- [37] M. T. Simons, J. A. Gordon, C. L. Holloway, D. A. Anderson, S. A. Miller, and G. Raithel, Using frequency detuning to improve the sensitivity of electric field measurements via electromagnetically induced transparency and Autler-Townes splitting in Rydberg atoms, *Appl. Phys. Lett.* **108**, 174101 (2016).
- [38] S. Rochester, Atom density matrix, <http://rochesterscientific.com/ADM/>.
- [39] F. Jia, J. Zhang, L. Zhang, F. Wang, J. Mei, Y. Yu, Z. Zhong, and F. Xie, Frequency stabilization method for transition to a Rydberg state using Zeeman modulation, *Appl. Opt.* **59**, 2108 (2020).
- [40] F. Jia, Y. Yu, X. Liu, X. Zhang, L. Zhang, F. Wang, J. Mei, J. Zhang, F. Xie, and Z. Zhong, Dispersive microwave electrometry using Zeeman frequency modulation spectroscopy of electromagnetically induced transparency in Rydberg atoms, *Appl. Opt.* **59**, 8253 (2020).
- [41] D. B. M. Auzinsh and S. Rochester, *Optically Polarized Atoms: Understanding Light-Atom Interactions* (Oxford University Press, Oxford, 2010).
- [42] D. A. Anderson, A. Schwarzkopf, S. A. Miller, N. Thaicharoen, G. Raithel, J. A. Gordon, and C. L. Holloway, Two-photon microwave transitions and strong-field effects in a room-temperature Rydberg-atom gas, *Phys. Rev. A* **90**, 043419 (2014).
- [43] M. T. Simons, A. H. Haddab, J. A. Gordon, and C. L. Holloway, A Rydberg atom-based mixer: Measuring the phase of a radio frequency wave, *Appl. Phys. Lett.* **114**, 114101 (2019).
- [44] M. Jing, Y. Hu, J. Ma, H. Zhang, L. Zhang, L. Xiao, and S. Jia, Atomic superheterodyne receiver based on microwave-dressed Rydberg spectroscopy, *Nat. Phys.* **16**, 911 (2020).